Research Article

Huda AlFannakh*, S. S. Arafat, and S. S. Ibrahim

Synthesis, electrical properties, and kinetic thermal analysis of polyaniline/polyvinyl alcohol - magnetite nanocomposites film

https://doi.org/10.1515/secm-2019-0020
Received Feb 05, 2019; accepted Jun 13, 2019

Abstract: Polyaniline-poly vinyl alcohol (PANI-PVA) conducting blends containing 15 wt% aniline were synthesized by in situ polymerization of aniline. Three-phase polymer blended nanocomposites with different contents of magnetite (5, 10 and 15 wt.%) were also synthesized. We measured the current-voltage (I-V) curves for the conducting blend and its magnetite nanocomposite. We also measured their thermal stability, and performed kinetic analysis through thermogravimetric analysis. We observed that the three phase nanocomposites showed enhanced electrical conductivity compared with that of the conductive blend, and no electrical hysteresis. The PVA/PANi blend was more stable above 350°C and the addition of Fe_3O_4 enhanced the thermal stability of the conductive blend. The apparent activation energy of the three phase nanocomposites was greater than those of both the pure PVA and PVA/PANi samples. These results suggest that such three phase nanocomposites could be used in a range of applications.

Keywords: Three-phase nanocomposite, Polyaniline-poly vinyl alcohol, Kinetic analysis, Thermogravimetric analysis, I-V characteristics, magnetite

1 Introduction

Magnetic nanoparticles have various characteristics that have drawn considerable research interest, in terms of both fundamental scientific studies and technological applications. Such applications have increased in recent decades to cover various medical and industrial fields. Ferro-fluids are used in audio speakers, magnetic recording media, and magnetic resonance imaging, and many relevant studies have been published [1–5].

Intrinsically conducting polymers (ICPs), are long range conjugated polymers with the ability to conduct an electrical current. ICP-based polymeric composites have many practical applications [6, 7], owing to their easy synthesis, low density, and controllable electric conductivity. Conferring magnetic properties to intrinsically non-magnetic ICPs has recently drawn the attention of many researchers [8]. ICP-based magnetic conducting polymer composites have a wide scope of applications. These applications extend from replacing conventional magnetic polymer-composites to more sophisticated electronic applications. Furthermore, such composites are regarded as attractive alternatives for microwave applications and electromagnetic interference shielding [9–13].

Polyaniline (PANI) is considered to be a particularly useful ICP because of its good chemical stability, relatively low cost, and ease of synthesis [14, 15]. Furthermore, it exhibits metallic conductivity. However, PANI has very poor mechanical and thermal stabilities in its conducting state [16]. This necessitates its preparation in a copolymer form. The problem of poor thermal stability of PANI alone can be solved by preparing PVA/PANI blends, and blending PANI with polyvinyl alcohol (PVA) is an effective solution [17, 18]. In addition, films prepared from PANI blended with polyvinyl alcohol (PVA) exhibit reasonable mechanical stability over a wide temperature range.

From a technical viewpoint, it is well known that physical properties of polymer composites tend to vary as a result of many processing factors, such as the matrix/filler interactions. Depositing a PANI polymeric matrix over magnetic ferrite particles is one way of promoting this interaction. This preparation technique not only effectively reduces the surface area but also enhances the physical properties [19, 20].

***Corresponding Author: Huda AlFannakh:** Physics Department, College of Science, King Faisal University (KFU), KSA; Email: halfannakh@kfu.edu.sa
S. S. Arafat: Physics Department, College of Science, King Faisal University (KFU), KSA; Physics Department, Faculty of Science, Fayoum University, Egypt
S. S. Ibrahim: Physics Department, Faculty of Science, Cairo University, Egypt

By incorporating a non-conductive filler during in situ polymerization of PANI, various ranges of conductivity have been obtained. In all cases, end-capped polymers were found to have higher electrical conductivity than that of the PANI/PVA blend alone. Thus, the loss in the electrical conductivity of PANI as a result of its blending with PVA can be compensated for by cross linking PANI chains over magnetite nanoparticles [21].

Generally speaking, various types of magnetic fillers can efficiently impart magnetic character to conductive polymer composites; however, ferrite nanomaterials are superior for this purpose [22, 23]. The success of the processing depends mainly on the compatibility between the filler and polymer. Magnetite as a magnetic filler is generally compatible with PANI [10], and also imparts good magnetic properties at a low loading level.

Previous work of Nagvenkar *et al.* has reported enhanced thermal conductivity of sonochemically synthesized iron nano-fluids. Ibrahim *et al.* [24] found that the dark current-voltage characteristics of three-phase multiwalled carbon-nanotube/polyaniline/magnetite composites were non-linear and showed rectification behavior. Khouloud *et al.* [25] studied the effects of nano-filler loading of surface modified Fe_3O_4 by polyaniline/epoxy nanocomposites in terms of their tensile, mechanical, and dielectric properties. They found that 3 wt% of filler enhanced the tensile strength and the glass transition temperature. A high charge transfer resistance was achieved through the use of 3 wt% of filler compared with that of pure epoxy. Other researchers have investigated two phase PANi/FeO_4 composites [26–36].

In the present work, we investigate the electrical and thermal stability of PVA/PANI blends and nanocomposites with magnetite nanoparticles. Our objective was to investigate the effects of magnetite nanoparticles on the electrical properties (I-V characteristic curve) and thermal stability of PVA/PANi blends. The model-free method was also used to estimate the activation energy of the PVA/PANi blend and its magnetite nanocomposite.

2 Experimental

2.1 Preparation of magnetite (Fe_3O_4) nanoparticles

Magnetite nanoparticles have been synthesized by controlled co-precipitation techniques [37, 38]. Ferrous chloride (99.99%) and ferric chloride (99.9%) were purchased from Merck - Sigma-Aldrich. A solution of ferrous chloride, ferric chloride in a molar ratio 1:2 was freshly prepared. Ammonia solution was then added dropwise under vigorous stirring and nitrogen sparging. Magnetite crystals were formed and precipitated; this powder was subsequently removed from the liquid phase with the aid of an external magnet. The powder was rinsed with deionized water and separated by centrifugation.

2.2 X-ray Diffraction Measurements of Fe_3O_4

X-ray diffraction (XRD) was performed on a Philips Pu 1390 channel control diffractometer with a Cu-K_α target and a filter of wavelength (λ = 1.791 Å). Measurements were acquired at 300 K using a power source 50 kV and 150 mA. X-ray diffractograms are plotted from data obtained from $2\theta = 10^\circ$ to $2\theta = 80^\circ$ at a rate of 2 min^{-1}.

2.3 Synthesis of PANI-PVA blends and PVA/PANi/Fe_3O_4 nanocomposite:

A 15-wt% PVA hydrogel was prepared by soaking PVA powder (Mw 130,000, >99% hydrolyzed Sigma-Aldrich) in distilled water for 4 h at room temperature. The preparation was completed by stirring the slurry at 70°C for a further 4 h. Finally, the hydrogel was allowed to cool down to ambient conditions.

Aniline hydrochloride (>99% Sigma-Aldrich) was dissolved portion-wise in the PVA hydrogel in a 1:1 ratio with PVA and the mixture was brought to 40°C with an ice bath. Magnetite powder was dispersed in the aniline/PVA hydrogel, then 1.0 g of ammonium persulphate (APS, ACS reagent >98% Sigma-Aldrich) was added to 40 mL of hydrochloric acid (1 M) and stirred. The APS solution was then added dropwise to the aniline/PVA hydrogel. A few minutes after injection of the oxidant, the solution turned bluish-green color. Over time, the color of the reaction mixture increased in strength. After 4 h of continuous stirring, the resulting greenish black thick gel was cast into clean Teflon molds and allowed to dry for 48 h at 30°C. Table 1 illustrates the sample code and the weight ratio contents for each sample.

Table 1: Samples code

Sample code	S0	S1	S2	S3
Fe_3O_4 wt.%	0	5	10	15

3 Results and discussion

3.1 X-ray Diffraction Analysis of Fe_3O_4

Figure 1 shows the X-ray diffraction pattern of Fe_3O_4 sample. The pattern revealed a single-phase crystalline structure. The phase purity was confirmed from the absence of unexpected peaks when the diffraction pattern was compared with the corresponding ICCD card No. [00-75-0449] as shown in the figure. The sample crystallized in the cubic unit cell of space group (Fd-3m). The lattice parameter (a) was calculated from the cubic symmetry by the simple relation: $a = d(h^2 + k^2 + l^2)^{1/2}$ and was found to be 8.3313 Å.

X-ray diffractograms of Fe_3O_4 showed relatively broad peaks indicating that the prepared samples crystallized on the nanometer scale. The crystallite size was calculated, assuming a spherical shape, with the Scherrer's formula: $L_{hkl} = k\,\lambda / \beta \cos\theta$, where L_{hkl} is the crystallite size, k is a constant (k = 0.89), λ is the wavelength of the X-ray target, β is the full width at half maximum (FWHM), and θ is the angle of diffraction. The calculated crystallite size was found to be 78 nm, which indicated that the particles were of nanometer size.

3.2 Electrical Properties (I-V Characterization)

The I-V characteristic curves of PVA/PANi blend and PVA/PANi/Fe_3O_4 nanocomposites were measured at different temperatures in the range from 30 to 110°C. Figure 2a shows the I-V characteristic curves for the blended sample (PVA/PANi). The blended sample exhibited a much higher electrical conductivity than that of pure PVA, which is consistent with previous studies [39–41]. A voltage ranging from −5 to +5 V was applied to the sample for all measurements. The I-V curves showed a degree of asymmetry between the positive and the negative sides of the applied voltage. The maximum current at 110°C was 1 mA whereas the lowest current at room temperature was 0.09 mA. The electrical current increased at higher temperatures, changing by an order of magnitude over the tested range.

The samples showed an electrical hysteresis during cycling of the voltage (from −5 to +5 V) at the same voltage steps and constant temperature (see Figure 2b). The hysteresis persisted even at high temperature.

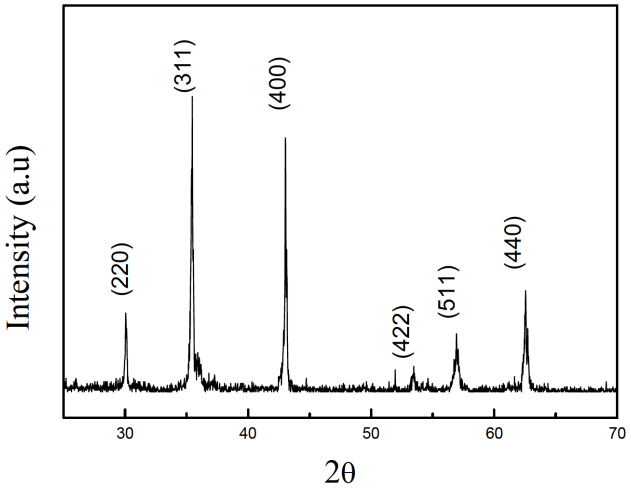

Figure 1: XRD patterns of Fe_3O_4 particles.

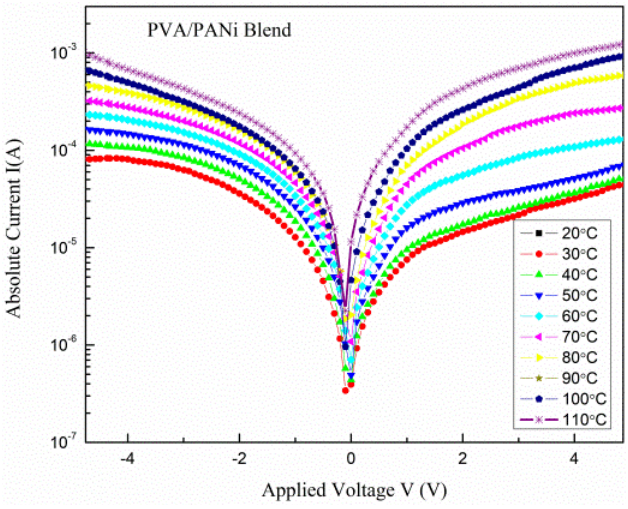

(a)

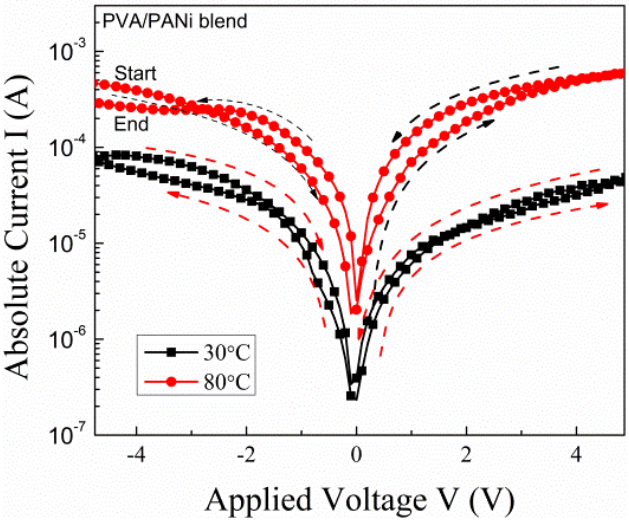

(b)

Figure 2: I-V characteristic curves for PVA/PANi blend sample a) at different temperatures b) cyclic runs at 30 and 80°C.

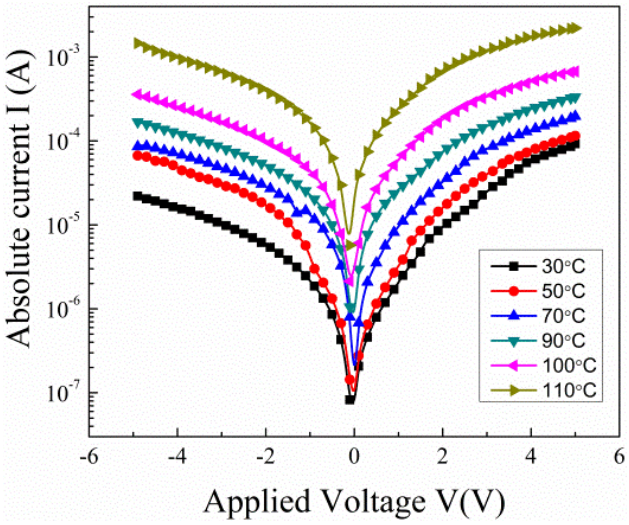

(a)

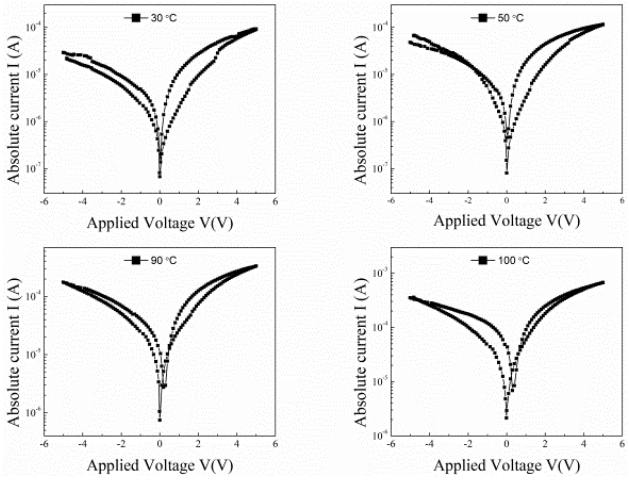

(b)

Figure 3: I-V characteristics for PVA/PANi/5 wt.% Fe_3O_4 blend nanocomposite a) at different temperatures b) cyclic runs at different temperatures.

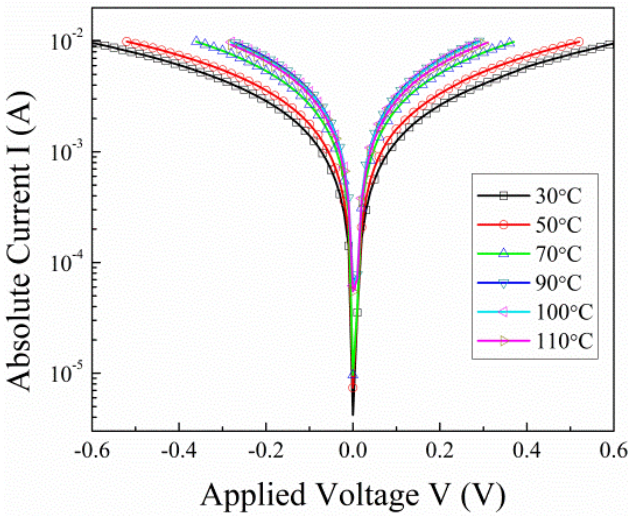

(a)

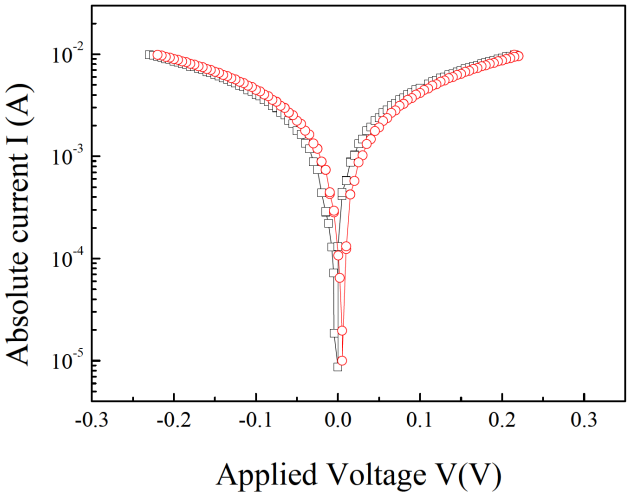

(b)

Figure 4: I-V characteristics of the PANi/PVA/10 wt% Fe_3O_4 blend nanocomposites a) at different temperatures b) cyclic run at 70°C.

Figure 3a and Figure 3b show the I-V curves for the PVA/PANi/5 wt% Fe_3O_4 nanocomposite sample and the cyclic behavior at different temperatures, respectively. The sample did not show any notable differences in its behavior compared with the PVA/PANi blend sample (Figure 3a). A hysteresis curve was present at all measuring temperatures, as shown in Figure 3b. This behavior can be explained by the absence of nanoparticles, which might improve the electrical properties of the nanocomposite. Furthermore, a nanoparticle content of 5 wt% did not improve conduction compared with that of the pure sample.

Figure 4 and Figure 5 show the effects of the addition of high contents of the magnetite nanoparticles (10% and 15%) on the I-V characteristics of the PANi/PVA conductive blend. During the in situ polymerization process, layers of the conductive blend formed on the magnetic nanoparticles which increased the homogeneity of the filler distribution. This capping layer also formed a three-dimensional network of a conductive blend and reduced the inhomogeneous region by reducing the formation of PVA islands through the bulk of the sample. In this way, the microstructure formed a good pathway for free charge carriers and reduced the accumulation of surface charges, which caused the cyclic I-V curves. For the high-filler content sample, the interstitial distances were reduced to provide additional conduction mechanisms, which increased the electrical conductivity. Notably, the flexibility of the samples (as shown in Figure 6) was maintained even at a 15 wt%

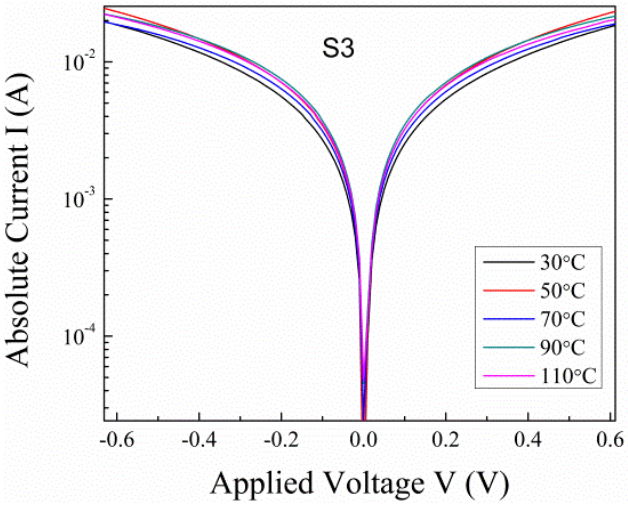

(a)

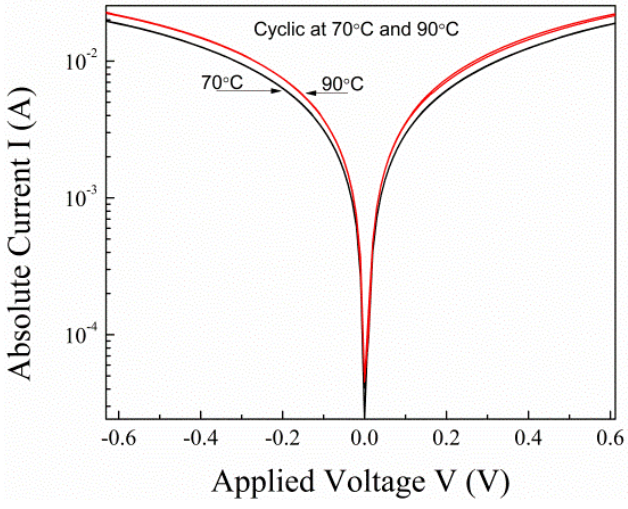

(b)

Figure 5: I-V characteristics for PANi/PVA/15 wt% Fe_3O_4 blend nanocomposites a) at different temperatures b) cyclic runs at 70 and 90°C.

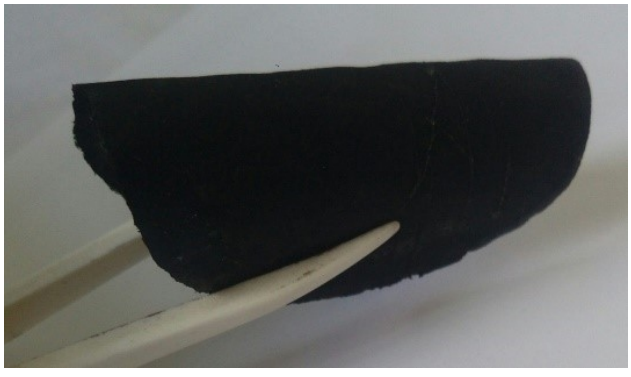

Figure 6: Photograph showing the elasticity of the three-phase conducting polymer nanocomposite.

content of nanoparticles in the polymer blend. Thus, we achieved a high electrical conductivity while retaining the mechanical flexibility of samples containing the magnetic materials.

We observed that the sample containing the highest weight percentage of Fe_3O_4 magnetic nanoparticles showed the highest current, and therefore the highest electrical conductivity [42]. This sample did not show any electrical hysteresis and the I-V curves were symmetric about zero voltage.

Figure 7 illustrates the nonlinear behavior during a complete cycle for the sample loaded with 5 wt.% Fe_3O_4 and the linear behavior for the 10 wt% and 15 wt% samples at 100°C.

We note that increasing the weight ratio of the magnetic filler caused the hysteresis to disappear, owing to the better sample homogeneity and the higher electrical conductivity of the nanocomposite. For the unloaded PVA/PANi blend sample, the presence of insulating polymer domains (PVA-islands) might have affected the appearance of the I-V hysteresis.

3.3 Thermogravimetric Analysis

Figure 8a illustrates the TGA decomposition curve (N_2 atmosphere and 10°C/min heating rate) for the temperature range from 60 to 500°C for PVA/PANi blend and PVA/PANi/Fe_3O_4 nanocomposite samples. Figure 8b shows the same curve focused to the range of the decomposition region (125 to 250°C). The effect of the Fe_3O_4 nanofiller on the thermal stability of the polymer is illustrated through a change in the decomposition rate (curve trend or slope) and the apparent shift of the on-set temperature for the first reaction. Figure 8c illustrates the dependence of the sample weight loss on the magnetite weight ratio at different temperatures. This figure illustrates the change in thermal stability owing to the addition of Fe_3O_4. For example, at 500°C, the weight loss is 43% lower owing to the addition of 15 wt% of the magnetic nano-filler.

3.3.1 Thermal stability

Figure 9a and Figure 9b illustrate the TGA decomposition curve and its 1st derivative for pure PVA and PVA/PANi blends respectively under a N_2 atmosphere at a heating rate of 10°C/min. For the PVA/PANi blend, we observed five decomposition regions in the temperature range from 25 to 500 °C, from the DTGA spectrum (Figure 9b). Thermal decomposition of the PVA polymers consisted of three

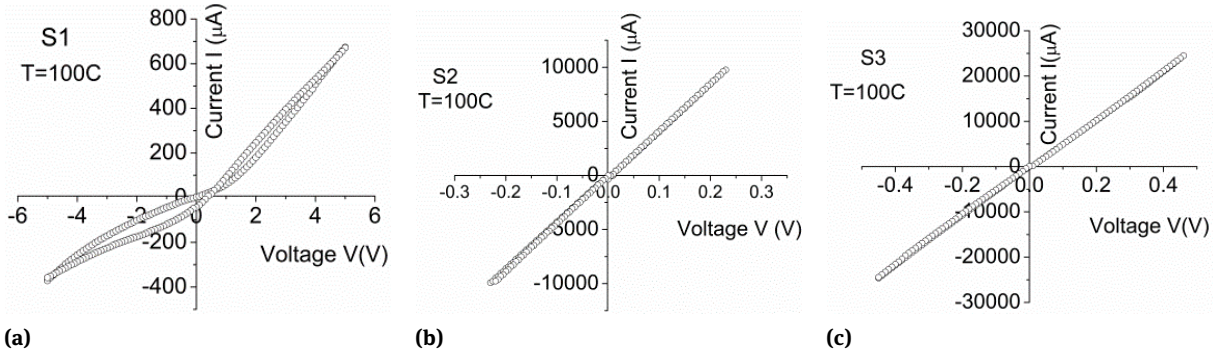

(a) (b) (c)

Figure 7: Nonlinear and linear I-V behavior for a) 5 wt% Fe_3O_4, b) 10 wt% Fe_3O_4, and c) 15 wt% Fe_3O_4.

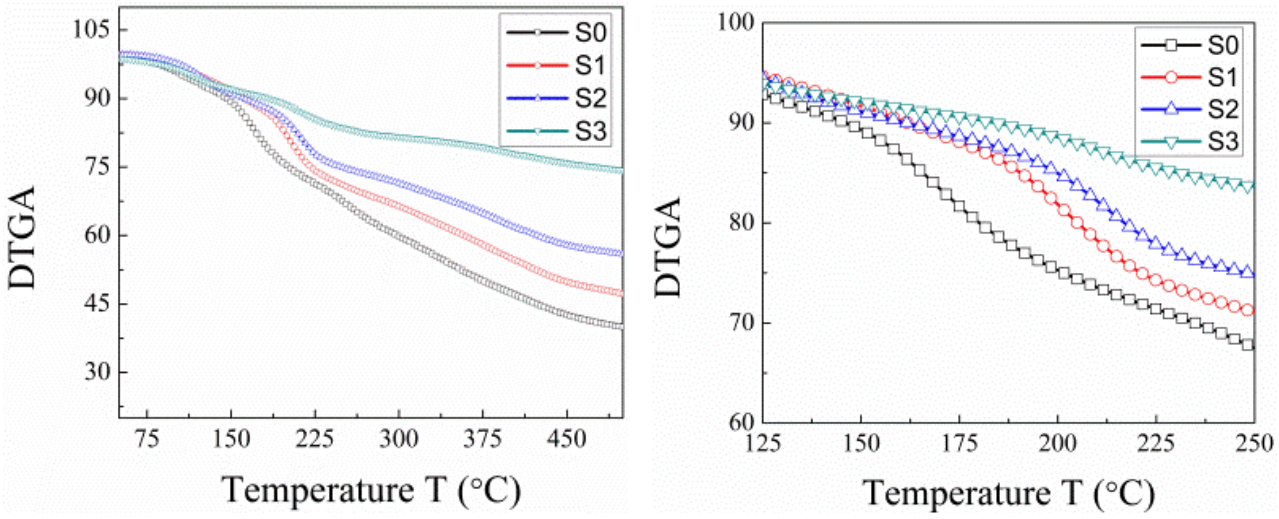

(a) (b)

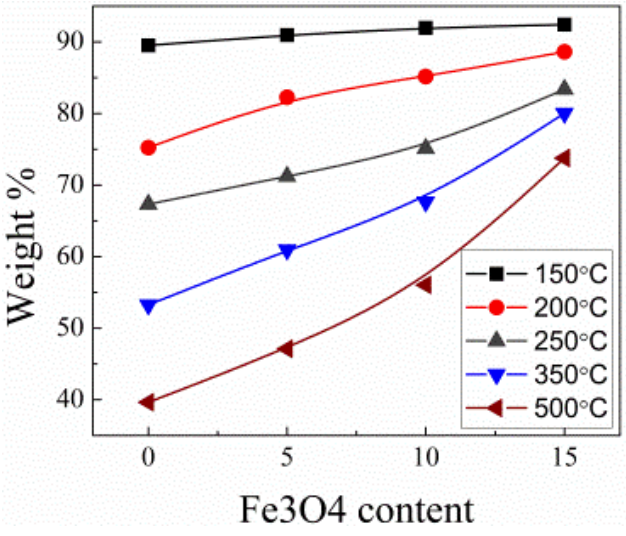

(c)

Figure 8: TGA curves for polymer blend and their Fe_3O_4 nanocomposite samples a) from 70 to 500°C b) from 125 to 250°C and c) Dependence of weight loss on magnetite weight ratio at different temperatures.

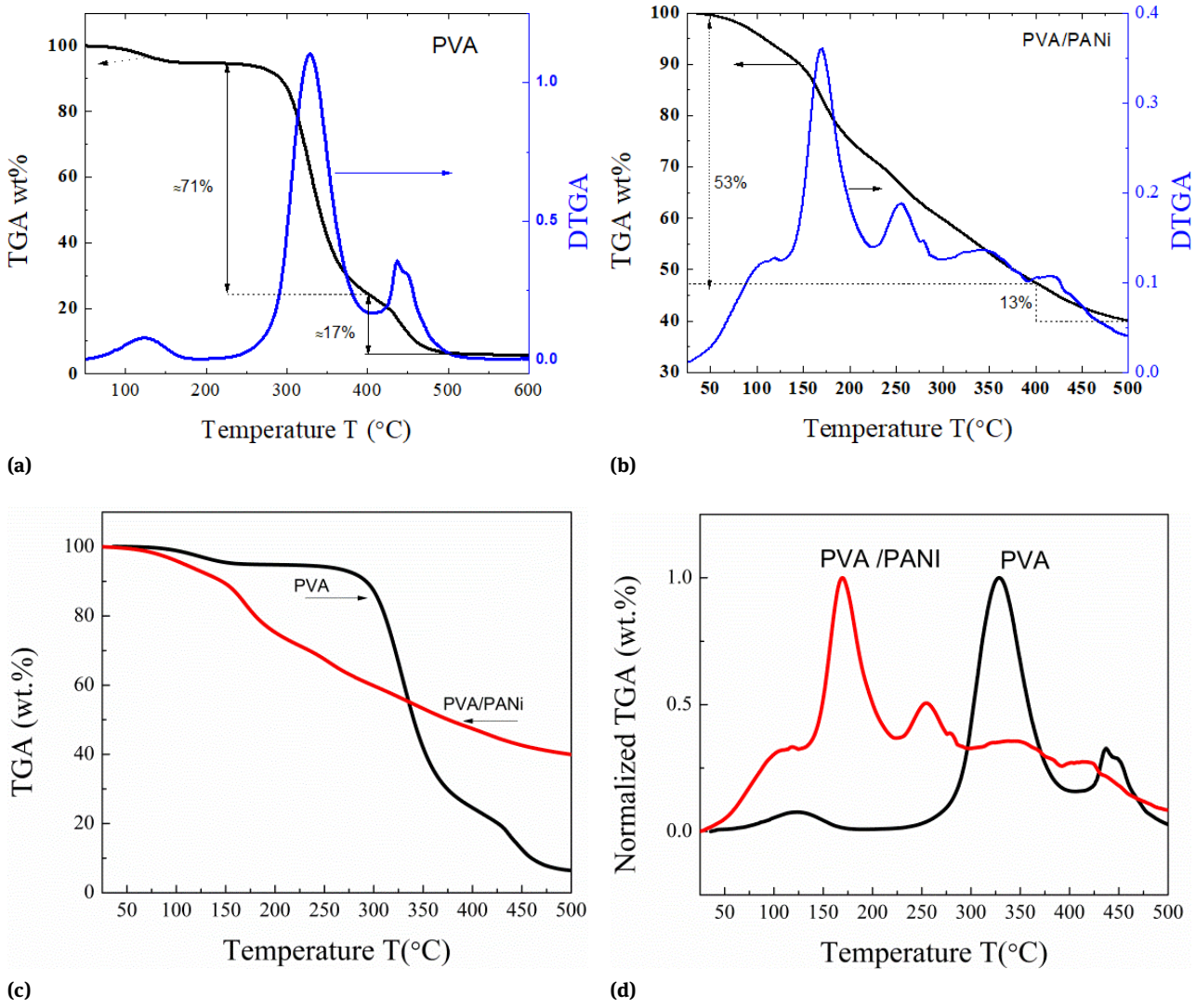

Figure 9: TGA and DTGA curves for a) pure PVA b) PVA/PANi blend, and a comparison of c) TGA and d) DTGA curves for pure PVA and polymer blend PVA/PANi.

degradation steps (Figure 9a). In the first decomposition stage of PVA, trapped water molecules were eliminated (at approximately 120°C); in the second stage (~330 °C) hydroxyl groups were eliminated. For the third stage (at approximately 450°C) a conjugated structure formed from the product of the second stage and carbonyl groups.

The thermal stability of PANi and its blends and composites depends on the method of synthesis and the type of dopant/blend [43, 44].

Figure 9-9c and Figure 9d represent a comparison between the decomposition behavior between pure PVA and polymer blend PVA/PANi. The thermal stability of the polymer blend (PVA/PANi) is less than that of the pure polymer (PVA) in the range below 350°C, but it is more stable in the range above 350°C (see Figure 9c for comparison) [45]. At 500°C was 6% of the sample remained for pure PVA but 40% remained for PVA/PANi conductive polymer blend. We note that the decomposition curve of the PVA/PANi polymer blend continued to decrease and did not show any clear stepwise decomposition except for features in the range 120–220°C. As for PVA, the decomposition of the first stage at 120°C appeared, whereas the two decomposition processes for PVA/PANi occurred in the temperature range 130–280°C, over which PVA showed no notable contributions. The features of PVA dehydration etherification, which has a maximum rate of decomposition at 330°C were almost absent from the conductive blend sample.

Figure 10a and Figure 10b show the 1st derivative of the TGA curves (DTGA) of PVA/PANi and the three-phase

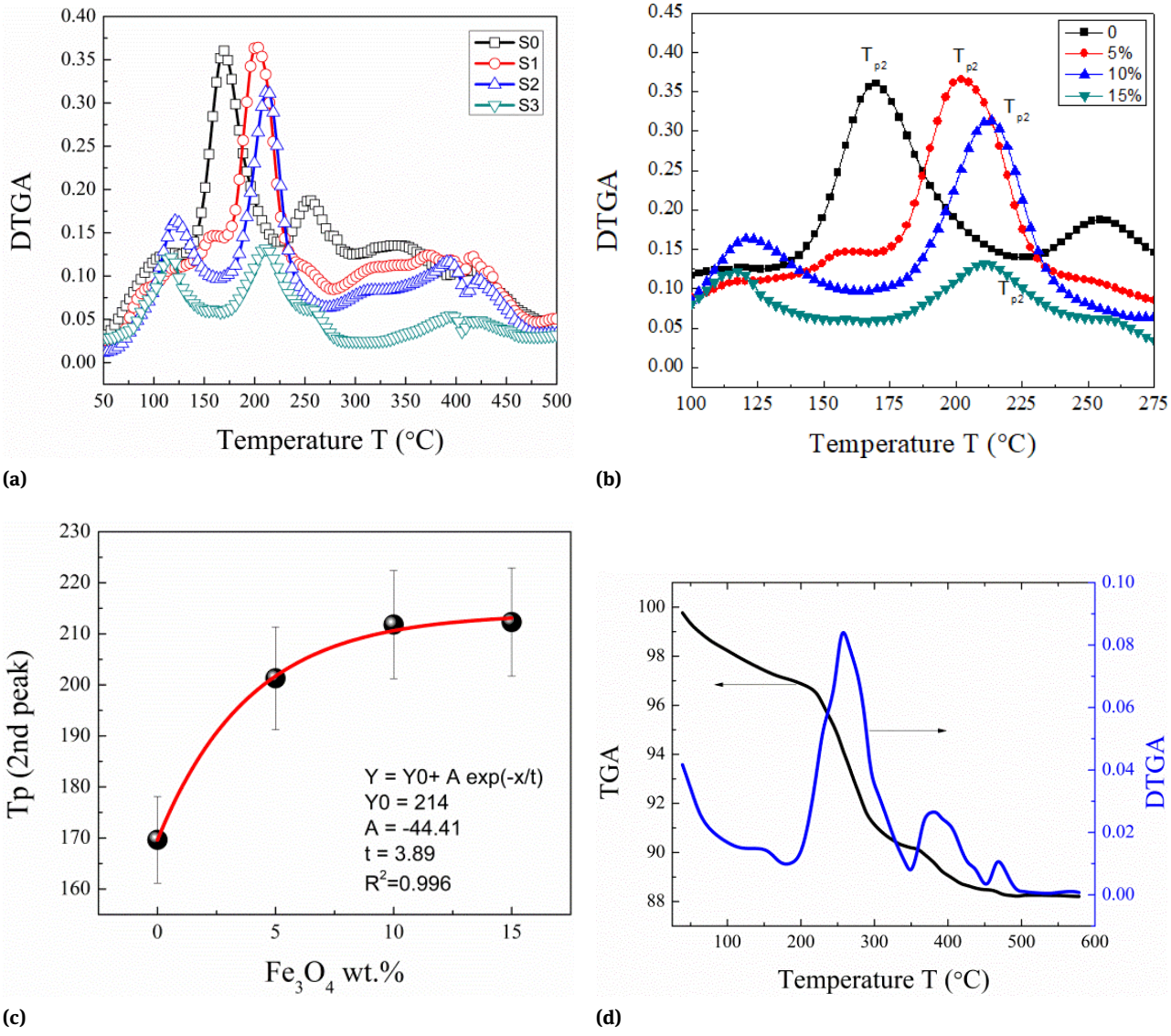

Figure 10: a) and b) DTGA curves for PVA/PANi blend and samples loaded with Fe_3O_4, c) Dependence of the second reaction peak position (T_{p2}) on the filler weight ratio, d) TGA and DTGA curves for Fe_3O_4 nanoparticles.

nanocomposite PVA/PANi/Fe_3O_4. The DTGA behavior indicated that the thermal stability of the conductive three phase nanocomposites increased with increasing Fe_3O_4 ferromagnetic nanoparticle content [46]. The thermal decomposition behavior of the three-phase nanocomposite samples depended on the weight ratio of the Fe_3O_4 magnetic nanoparticles.

The effects of Fe_3O_4 were pronounced over the main reaction region (50–350°C), which shifted to higher temperature owing to the addition of magnetite. The decomposition process owing to the conjugated structure, formed from the second stage and carbonyl groups, was not notably affected by the addition of Fe_3O_4 nanoparticles.

By considering the reaction at T_{p2} =170°C for PVA/PANi (*i.e.*, the second reaction) as the main reaction of the conductive blend, we observed a shift of the reaction peak to higher temperatures as the weight ratio of Fe_3O_4 increased (Figures 10a and 10b). The distance between filler nanoparticles decreased as the filler weight ratio increased. At a certain percolation threshold of the filler, a three-dimensional network formed, which increased the thermal resistance of the composite. The magnetic nanoparticles act as dispersive centers for phonons, affecting the heat transfer of the unexposed region of the sample. This effect delays the decomposition process of the polymer blend.

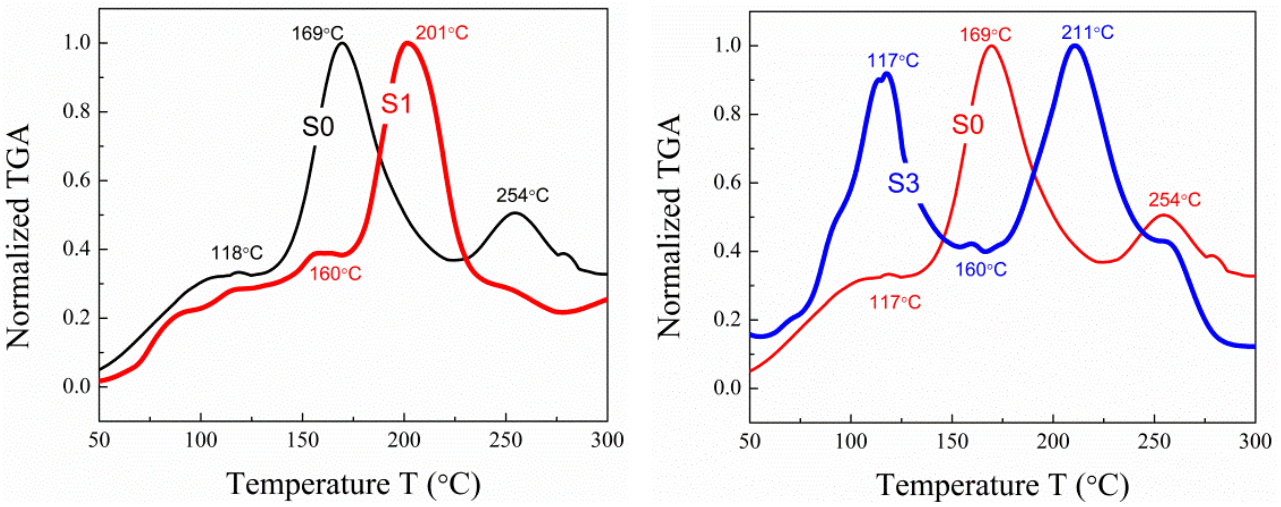

Figure 11: DTGA curves for PVA/PANi blend (S0) and 5 wt. (S1) and 15 wt% (S3) Fe_3O_4 loaded samples a) comparison between S0 and S1 b) comparison between S0 and S3.

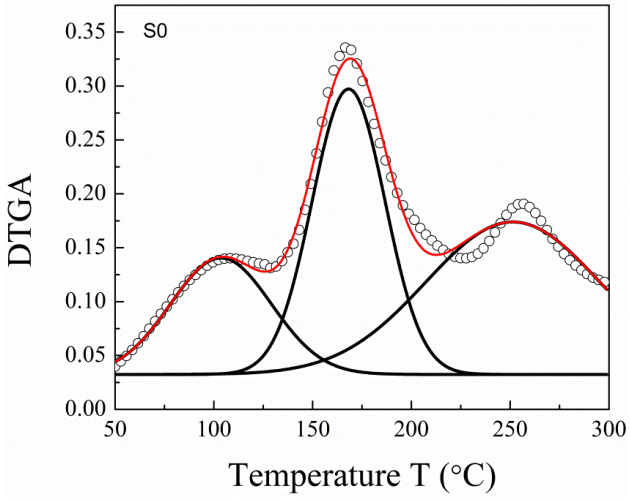

Figure 12: DTGA curve for PVA/PANi blend sample, fitting curve (read) and peak separation (black).

Figure 10c shows the temperature dependence of the second reaction peak position (T_{p2}) on the filler weight ratio in addition to exponential fits to the experimental data. The TGA curve of the Fe_3O_4 nanoparticles (Figure 10d), showed that the weight loss was less than 20% up to 600°C and a DTGA peak corresponding to the maximum decomposition rate appeared close to 280°C, which was absent in the three phase samples.

Figure 11a and Figure 11b compare S_0 against S_1 and S_3, respectively. We observed that, the third decomposition process for S_0 (at 254°C) became a shoulder of both S_1 and S_3, whereas the second decomposition peak shifted from 169 to 201°C for S_1 and 211°C for S_3.

3.3.2 Kinetic thermal analysis

Next, we predicted the apparent activation energy based on kinetic thermal analysis. For this purpose, we compare only the pure PVA/PANi blend samples with the three-phase PVA/PANI/Fe_3O_4 (10 wt.%) sample.

We noted an overlap between the decomposition processes, which became progressively more complex in the case of the PVA/PANi/Fe_3O_4 magnetic blend nanocomposite. To address this problem, we used a mathematical method to separate the closely overlapping interactions in Origin Lab 0.8, and then studied the kinetics of the decomposition of each process separately. This method allowed us to use high-resolution kinetic analysis by separating and considering each reaction as a one-step reaction or 1st order reaction. This analysis is a valid comparative approach to identifying the effects of fillers on the polymer or polymer blend.

Many models have been used to calculate activation energy based on kinetic thermal analysis for non-isothermal decomposition. In the case of model-free methods for estimating activation energies, we avoid the problem of identifying a suitable kinetic model for the reaction. In some cases, we obtained more than one model to be applied for a single reaction, which may cause conflicting results. In the case of studying the effect of fillers on the ther-

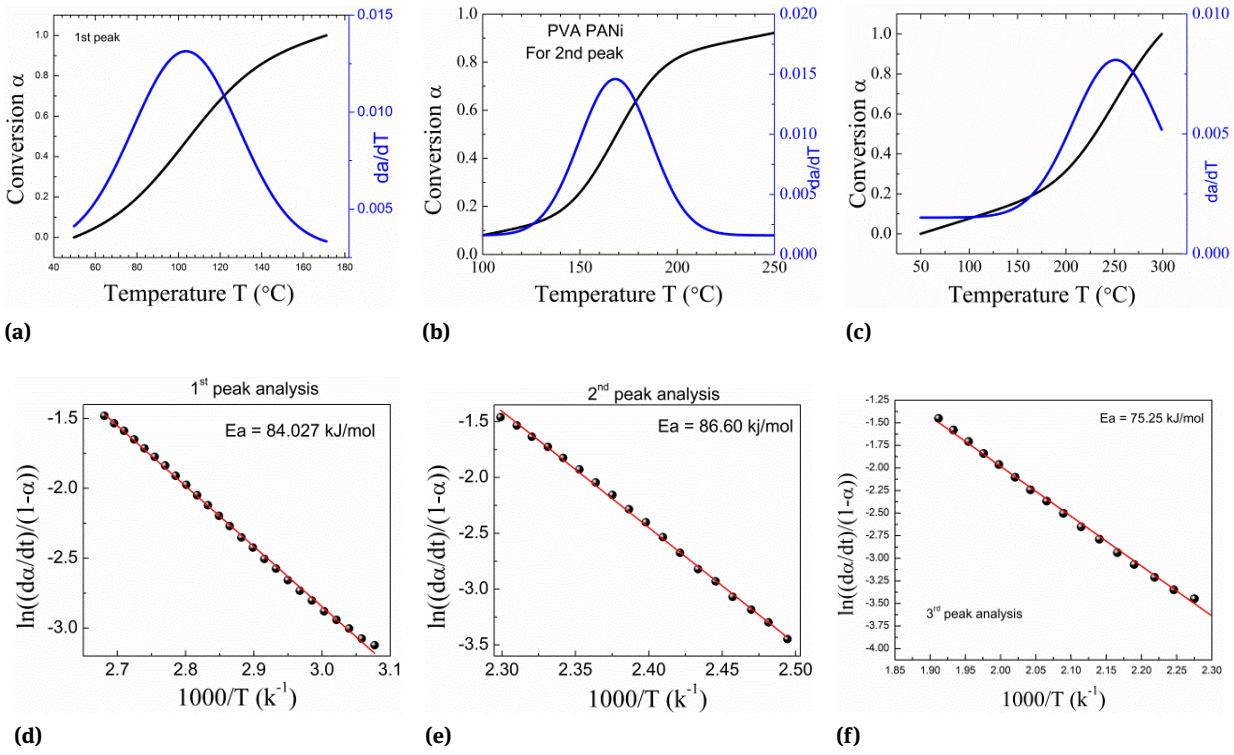

Figure 13: Conversion rate and its 1st derivative for the a) first reaction, b) second reaction, and c) third reaction, and ln[(dα/dt)/(1 - α)] vs. 1/T relation for the d) first reaction, e) second, reaction and f) third reaction of the PVA/PANi blended sample.

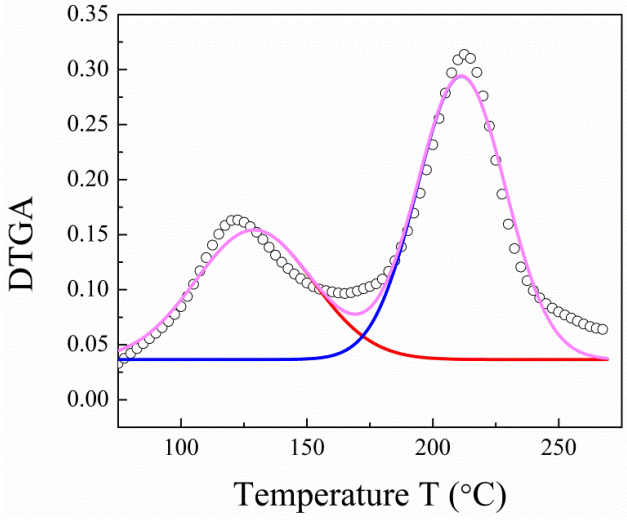

Figure 14: DTGA curve for PVA/PANi/Fe_3O_4 blend nanocomposite loaded with 10 wt.% of Fe_3O_4 sample, fitting curve (pink), and peak separation (red and blue).

mal behavior of composite/nanocomposite materials, the model-free approach is a useful short cut.

The differential form of the rate equation can be expressed in terms of the conversion factor α as:

$$\frac{d\alpha}{dt} = k(T)f(\alpha) \tag{1}$$

where $k(T)$ and $f(\alpha)$ are the rate constant and reaction model function, respectively. The reaction model function can take several mathematical forms. Each form of $f(\alpha)$ depends on the type of reaction and the physical mechanism of the reaction. Equation (1) can take the form:

$$\frac{d\alpha}{dt} = A \exp\left(\frac{-E}{RT}\right) f(\alpha) \tag{2}$$

where A is the pre-exponential factor, E is the apparent activation energy and R is the gas constant. These three parameters are known as the kinetic triplet, and are used to describe thermal decomposition analysis for a substance under examination.

By considering the reaction in our case to be a first order reaction, f(α) = 1 - α and equation (2) can be rewritten as:

$$\ln\left(\frac{\left(\frac{d\alpha}{dT}\right)}{(1-\alpha)}\right) = \frac{A}{\beta} - \frac{E_a}{R\,T} \tag{3}$$

The kinetic triplet components can be determined by plotting ln[(dα/dT)/(1-α)] vs. 1/T .

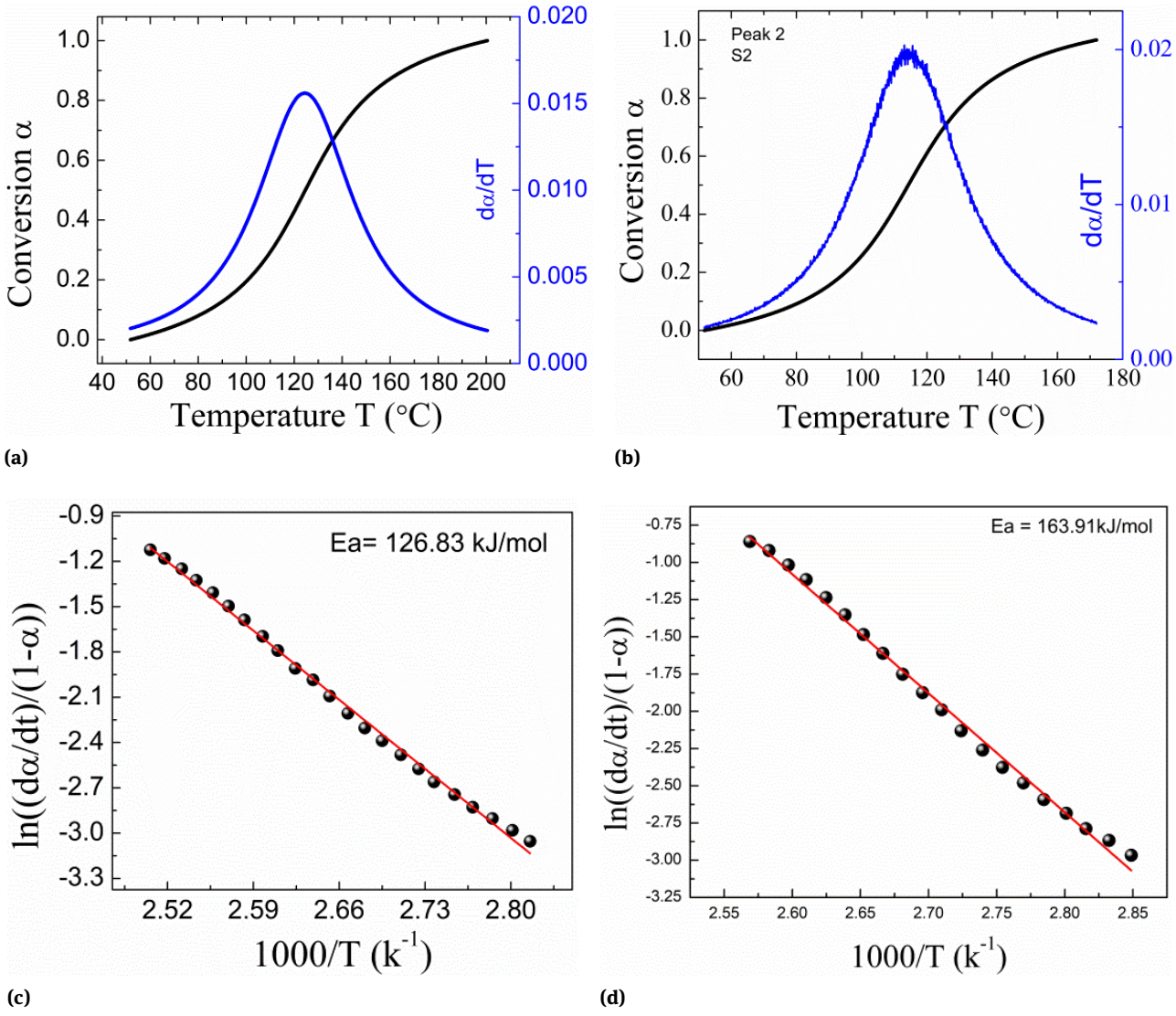

Figure 15: Conversion rate and its 1st derivative for the a) first reaction and b) second reaction, and ln[(dα/dt)/(1 - α)] vs.1/T relation for the c) first reaction, and d) second reaction for the PVA/PANi/10 wt.% Fe_3O_4 nanocomposite.

The iso-conversional method represents the main principal of the model-free approach. In this method, the reaction rate is considered to be a function of temperature only (*i.e.*, α is constant), giving:

$$\frac{(ln(d\alpha/dt))}{dT^{-1}} = \frac{d(\ln(k(T))}{dT^{-1}} + \frac{df(\alpha)}{dT^{-1}} = -\frac{E_a}{R} \qquad (4)$$

This equation can be used to determine the kinetic triplet in the case of a single heating rate. This can be performed by finding the 1st derivative of α with time at the point where the first derivative of α with temperature is zero. Hence, equation (4) can be used to predict the E_α without any information of the reaction model. Note that the basic assumption of this method is the applicability of Eq. (2) to the individual extent of conversion for the temperature region related to this conversion.

Figure 12 shows the DTGA curve for PVA/PANi blend sample and the main three peaks corresponding to the reactions involved between 50 and 300°C. OriginLab software was used to separate the complex overlapped TGA spectrum into three separate peaks.

The TGA curve corresponding to each separated peak was found mathematically and its conversion curve was calculated. Figures 13a–13c shows the conversion curves and their 1st derivatives for each of the three separated peaks. Each reaction region was analyzed separately by the Redfield method for kinetic analysis to determine the apparent activation energy for each reaction. Figures 13d

to 13f illustrates the relation between ln[(dα/dt)/(1 - α)] vs.1/T and the linear fitting for each reaction region. The activation energies for the three-reaction region were 84.0, 86.6, and 75.3 kJ/mol.

Wang *et al.* [47] reported on a kinetic analysis of PANi and PANi/ZrO_2. They determined the activation energies for both samples through Friedman and Ozawa–Flynn–Wall methods. The activation energy predicted by PANI was approximately 81.8 kJ/mol. The average activation energy in our work was 81.3 kJ/mol, which is very close to that predicted by Wang [47].

For the three-phase nanocomposite sample (PVA/PANi/Fe_3O_4) containing 10% Fe_3O_4, we applied the same method as described above. Figure 14 shows the DTGA curve for the 10 wt.% PVA/PANi/Fe_3O_4 sample in the temperature range from 50 to 300°C. This temperature range included only two reaction peaks. The complex overlapped peaks separated into two single step peaks and their corresponding TGA data were calculated. Both the conversion and its 1st derivative were calculated and are represented in Figures 15a and 15b, respectively. Figure 15c and Figure 15d shows the relationship between ln[(dα/dt)/(1 - α)] vs.1/T and the linear fitting for each reaction region. The activation energies for the two reaction regions were 126.8 and 163.9 kJ/mol.

The results for the activation energy indicate that the magnetite nanoparticles have a pronounced effect on the thermal state of the composite where the activation energy nearly doubled. Hence, interactions between the magnetite nanoparticles and the polymer mixture were created. We posit that the connection and formation of polymer blend on the surface of the nanoparticles produced physical interactions, such as an energy of adhesion. The resulting granules of material resulted in the surrounding polymeric structure behaving as one unit. Magnetite nanoparticles dispersed phonons and protected the adhesive polymer blend against decomposition. These nanoparticles also absorbed a large amount of thermal energy, reducing the chance of polymer chains decomposition.

4 Conclusions

We measured I-V characteristic curves, thermal stability, and kinetic thermal analysis of conducting polymer blend PVA/PANI and PVA/PANi/Fe_3O_4 nanocomposites. For the PVA/PANi conductive blend loaded with 10 wt% and 15 wt% Fe_3O_4, no electrical hysteresis appeared, whereas hysteresis appeared in the I-V characteristics of PVA/PANi and 5 wt% Fe_3O_4 samples. The addition of magnetite to the PVA/PANi conducting blend had a notable effect on the thermal decomposition curve of the samples. The main reaction peak of the polymer blend shifted to higher temperature. For a high Fe_3O_4 content sample, three dimensional networks formed and contributed to higher thermal resistance of the three-phase nanocomposite. The magnetite nanoparticles had a notable effect on the thermal state of the blend nanocomposite where the activation energy increased to nearly double its original value. Magnetite nanoparticles dispersed the phonons and protected the adhesive polymer blend against decomposition. The magnetite nanoparticles absorbed a large amount of thermal energy, reducing the chance of polymer chain decomposition.

Acknowledgement: This work was supported by Dean of Scientific Research (DSR), King Faisal University (KFU), Saudi Arabia (research project No. 180114). The authors would like to thanks Dr. Salem Gaballah, Cairo University, for his helpful advice on sample preparation and manuscript revision. We would also like to thank the Department of Physics, College of Science, King Faisal University for providing the necessary resources for conducting this work. We thank Andrew Jackson, PhD, from Edanz Group (www.edanzediting.com/ac) for editing a draft of this manuscript.

References

[1] Zaibudeen AW, Philip J. *Sens. Actuators B-Chem.* 2018, 255, 720–728.
[2] Anushree C, Philip J. *Colloids and Surf. A* 2019, 567, 193–204.
[3] Brojabasi S, Mahendran V, Lahiri BB, Philip J. *Opt. Commun.* 2015, 342, 224–229.
[4] Laskar JM, Philip J, Raj B. *Phys. Rev. E* 2010, 82, 021402.
[5] Laskar JM, Philip J, Raj B. *Phys. Rev. E* 2008, 78, 031404.
[6] Inzelt G. *Conducting Polymers: A New Era in Electrochemistry* 2008, 265–269.
[7] Shi Y, Peng L, Ding Y, Zhao Y, Yu G. *Chem. Soc. Rev.* 2015, 44, 6684–6696.
[8] Naarmann H. *Ullmann's Encyclopedia of Industrial Chemistry* 2000.
[9] Wang Y, Jing X. *Polymers for advanced technologies* 2005, 16, 344–351.
[10] Lyu J, Zhao X, Hou X, Zhang Y, Li T, Yan Y. *Compos. Sci. and Technol.* 2017, 149, 159–165.
[11] Faisal M, Polyaniline-Coated Inorganic Oxide Composites for Broadband Electromagnetic Interference Shielding, High-Performance Materials and Engineered Chemistry, Apple Academic Press, 2018, pp. 95–134.
[12] Bora PJ, Vinoy K, Ramamurthy PC, Madras G. *Compos. Commun.* 2017, 4, 37–42.

[13] Zhao H, Hou L, Bi S, Lu Y. *ACS Appl. Mater. Interfaces* 2017, 9, 33059–33070.
[14] Bhadra S, Khastgir D, Singha NK, Lee JH. *Prog. Polymer Sci.* 2009, 34, 783–810.
[15] Shown I, Ganguly A, Chen LC, Chen KH. *Energy Sci. Eng.* 2015, 3, 2–26.
[16] Simões FR, Bulhões LO, Pereira EC. *Polímeros* 2009, 19, 54–57.
[17] Li J, Li Y, Song Y, Niu S, Li N. *Ultrason. Sonochem.* 2017, 39, 853–862.
[18] Bhadra J, Al-Thani NJ, Madi NK, Al-Maadeed MA. *Arab. J. Chem.* 2017, 10, 664–672.
[19] Fu S-Y, Feng X-Q, Lauke B, Mai Y-W. *Compos. B Eng.* 2008, 39, 933–961.
[20] Jang J, University of Delaware, 2012.
[21] Bhadra J, Sarkar D. 2010.
[22] Arora R, Mandal UK, Sharma P, Srivastav A. *Mater. Today* 2015, 2, 2767–2775.
[23] Vinod S, Philip J. *J. Mol. Liq.* 2018, 257, 1–11.
[24] Ibrahim A, Abdel-Aziz MH, Zoromba MS, Al-Hossainy AF. *Synth. Met.* 2018, 238, 1–13.
[25] Jlassi K, Radwan AB, Sadasivuni KK, Mrlík M, Abdullah AM, Chehimi MM, Krupa I. *Sci. Rep.* 2018, 8, 13369.
[26] Qiao M, Lei X, Ma Y, Tian L, Su K, Zhang Q. *Ind. Eng. Chem. Res.* 2016, 55, 6263–6275.
[27] Liu P, Huang Y, Yang Y, Yan J, Zhang X. *J. Alloy Compd* 2016, 662, 63–68.
[28] Mondal S, Rana U, Malik S. *J. Phys. Chem. C* 2017, 121, 7573–7583.
[29] Wu Q, Chen M, Chen K, Wang S, Wang C, Diao G. *J.Mater. Sci.* 2016, 51, 1572–1580.
[30] Yang L, Cai H, Zhang B, Huo S, Chen X. *Mater. Res. Express* 2018, 5, 025304.
[31] Kong Y, Wu T, Wu D, Zhang Y, Wang Y, Du B, Wei Q. *Anal. Methods*, 2018, 10, 4784–4792.
[32] Trung VQ, Trang NT, Thi TM, Vorayuth K, Nghia NM, Tuan MA. Mater. Trans. 2018, 59, 1095–1100.
[33] Bahadur A, Iqbal S, Shoaib M, Saeed A. *Dalton Trans.* 2018, 47, 15031–15037.
[34] Hou J, Zhang L, Qiu H, Duan W, Wang X, Wan X, Du X. *J. Mater. Sci. Mater. Electron.* 2017, 28, 9279–9288.
[35] Diantoro M, Pradhana D, Mustikasari A, Kusumawati A, Taufiq A, Mufti N, Nur H, IOP Conference Series: Materials Science and Engineering, IOP Publishing, 2017, pp. 012062.
[36] Hosseinian A, Hosseinzadeh-Khanmiri R, Ghorbani-Kalhor E, Abolhasani J, Babazadeh M, Vessally E. *Nano* 2017, 12, 1750016.
[37] Gnanaprakash G, Philip J, Jayakumar T, Raj B. *J. Phys. Chem. B* 2007, 111, 7978–7986.
[38] Petcharoen K, Sirivat A. *Mater. Sci. Eng. B* 2012, 177, 421–427.
[39] Van Etten EA, Ximenes ES, Tarasconi LT, Garcia IT, Forte MM, Boudinov H. *Thin Solid Films* 2014, 568, 111–116.
[40] Krishnan K, Aono M, Tsuruoka T. *J. Mater. Chem. C* 2018,6, 6460-6464
[41] Bhadra J, Sarkar D. *Bull. Mater. Sci.* 2010, 33, 519–523.
[42] Long Y, Chen Z, Duvail JL, Zhang Z, Wan M. *Physica B: Condens. Matter* 2005, 370, 121–130.
[43] Yu Y, Che B, Si Z, Li L, Chen W, Xue G. *Synth. Met.* 2005, 150, 271–277.
[44] Ginic-Markovic M, Matisons JG, Cervini R, Simon GP, Fredericks PM. *Chem. Mater.* 2006, 18, 6258–6265.
[45] Shahi M, Moghimi A, Naderizadeh B, Maddah B. *Scientia Iranica* 2011, 18, 1327–1331.
[46] Ghanbari D, Salavati-Niasari M, Ghasemi-Kooch M. *J. Ind. Eng. Chem.* 2014, 20, 3970–3974.
[47] Wang S-X, Tan Z-C, Li Y-S, Sun L-X, Li Y. *J. Therm. Anal. Calorim.* 2008, 92, 483–487.